Acta Physicae Superficierum • Vol VII • 2004

EXPLORING ARTIFICIAL MAGNETISM FROM THIN FILMS TO NANOSTRUCTURES

C. RAU

Department of Physics and Astronomy
Rice Quantum Institute
Center for Nanoscale Science and Technology
Rice University, Houston, TX 77251, USA

Abstract. Surface, interface and bulk properties of artificially structured, new magnetic materials play a fundamental role in modern science and technology. From thin films to patterned magnetic nano-structures, these magnetic materials and systems can be utilized in many electrical and electronic devices.

Using highly surface sensitive techniques, electron capture spectroscopy (ECS), angle- and energy-resolved, spin-polarized ion-induced electron and Auger emission spectroscopy (SPEES) and scanning ion microscopy with polarization analysis (SIMPA), surface and interface magnetic order, short- and long-ranged magnetic order, magnetic anisotropy and critical behavior of ultra thin, patterned and continuous, macro- and nano-magnetic systems are investigated. All systems are well characterized by using Auger electron spectroscopy, low and high energy electron diffraction and scanning tunneling microscopy.

For several systems, surface and interface-enhanced magnetic order, 4*d*-ferromagnetism in two dimensions (2D), novel, non-universal surface critical behavior and magnetic anisotropies are found. Using SPEES, fundamental, element-specific information on layer-dependent electronic and magnetic properties of surfaces and interfaces is obtained. These findings are of paramount importance for a deeper and fundamental understanding of 2D ferromagnetism in thin films and nano-structures.

SIMPA enables us to study and fabricate *in situ* nano-structured, 3D, 2D and 1D magnetic elements and systems to be used for ultra-high density magnetic data storage, read heads, magnetic sensors and spin-electronic devices. SIMPA allows for detailed observations of the internal structure of magnetic domains and domain walls by providing high resolution, spatially- and spin-resolved maps of the orientation and magnitude of the surface electron spin polarization, which directly reveals the non-uniform behavior of the magnetization at the surface of magnetic domains. SIMPA is also utilized for studies on the dependence of magnetic domain structures on interlayer magnetic couplings as well as for studies on various magnetic vortex and antivortex configurations.

1. Introduction

For several decades, magnetic phenomena at surfaces, interfaces and in ultra-thin films receive great attention. This arises from the fact that magnetic materials serve as nearly ideal systems to explore basic concepts in theoretical physics, such as phase transitions and critical behavior of thermodynamic quantities in two or three dimensions. Moreover, the intense and broad scientific interest also stems from the fact that the development of new electronic and magnetic systems and devices of dimensions in the submicron region requires a fundamental understanding of topmost surface, interface layer and thin film electronic properties [1–4].

Recent scientific and technological advances have opened the way to exciting new opportunitites in the fabrication and characterization of novel, epitaxial, single- and multi-component, artificially structured magnetic systems of great scientific and economic importance (ultra-high density magnetic storage media, such as non-volatile magnetic RAM, miniaturized magnetic reading and writing heads, magnetic sensor arrays, etc.) [5, 6].

For the investigation of surface magnetic structures, we use ion-induced capture or emission of spin-polarized electrons from magnetic surfaces, which are powerful means for probing various surface properties, in particular surface magnetic properties. Electron capture spectroscopy (ECS) and spin-polarized electron emission spectroscopy (SPEES) permit the detection of the long-ranged and short-ranged electron spin polarization (ESP) existing at magnetic surfaces with extreme surface sensitivity [7–9]. Using scanning of a highly focused ion beam at surfaces of patterned and continuous magnetic systems and measuring the ESP of ion-induced emitted electrons, scanning ion microscopy with polarization analysis (SIMPA) enables us to detect the spatially and spin-resolved magnitude and orientation of the surface magnetization of magnetic domain and domain wall structures [10].

2. Experimental

Experimental details on ECS, SPEES and SIMPA are given in Refs. [7–10]. ECS allows us to study long-ranged (LRFO) and short-ranged (SRFO) ferromagnetic order at surfaces of magnetic materials. The physical process in ECS is the capture of one or two spin-polarized electrons during grazing-angle surface reflection of fast ions. For 150 keV deuterons and for an angle of incidence of 0.2° of the ions, the distance of closest approach to the reflecting surface amounts to 0.1 nm (Fig. 1: full line), and the ions probe spin-polarized electron densities of state at the *topmost* surface layer. LRFO is detected by exploiting one electron capture processes ($D^+ + e^- = D^0$) [7, 8]. SFRO is detected by exploiting two-electron capture processes ($H^+ + 2e^- = H^-$ or $D^+ + 2e^- = D^-$) [10]. It is found that at Ni(hkl) surfaces, SRFO exists even at $2T_{Cs}$ (T_{Cs} – surface Curie temperature) [11].

In angle- and energy-resolved SPEES, small angle surface scattering of energetic (5–150 keV) ions (H^+, He^+ or Ne^+) is utilized to study the emission of spin-polarized secondary and Auger electrons as a measure of LRFO. Fig. 1 illustrates ion trajectories for various scattering angles α. Varying α from 0.2° up to 45° allows us to vary the *probing depth* from the *topmost* surface layer to interface and deeper layers, allowing us to perform magnetic depth profiling. The ESP of secondary/Auger electrons emitted along the surface normal is detected by using an einzellens system and Mott detectors [9]. The ESP is defined by $P = (n^+ - n^-)/(n^+ + n^-)$ with n^+ and n^- being the numbers of majority- and minority-spin electrons [8]. $P > 0$, therefore, is related to a predominance of majority-spin electrons (ESP parallel to the total magnetization M), and $P < 0$ refers to a predominance of minority-spin electrons (ESP antiparallel to the total M).

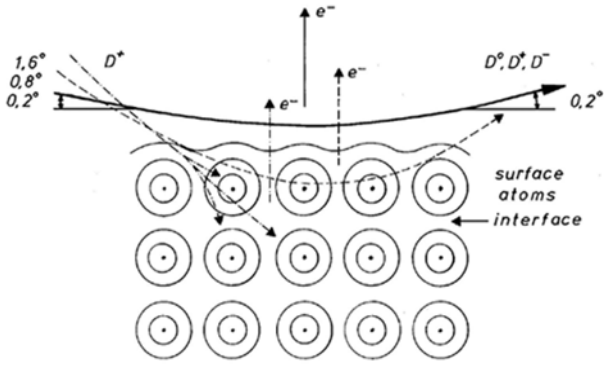

Fig. 1: Scheme illustrating the ion trajectories (for scattering angles α of 0.2°, 0.8° and 1.6°, the emission of ion-induced electrons and the surface potential plotted on a plane perpendicular to the surface plane.

In SIMPA a microfocused (min. spot size 35 nm) 6–30 keV Ga^+ ion beam is scanned across a magnetic or nonmagnetic surface of a sample causing the ion-induced emission of spin-polarized or non-spin-polarized electrons. A magnetic image is obtained by rastering the ion beam across the magnetic surface. By using an extraction lens system and a Mott detector, the orientation and magnitude of P of the electrons is analyzed. The SIMPA technique offers some unique advantages compared to many other magnetic imaging techniques, because of its capability to produce vectorial maps of M by directly measuring the spatially resolved vector orientation and magnitude of P [10, 12]. For the deposition of magnetic films, atomically clean, flat substrate crystals are prepared in a target preparation chamber operating in the low 10^{-10} mbar region. The films are deposited by using electron beam evaporation [7, 8].

3. Results and Discussion

ECS was most successfully applied to investigate the existence of LRFO existing at the *topmost* surface layer of various bulk ferromagnetic, antiferromagnetic and paramagnetic single-crystalline metals. It is found that the ESP at fcc Ni(hkl) surfaces is predominantly negative, indicating a predominance of so-called minority spin electrons as predicted by various band structure calculations [7, 8]. The ESP at Ni(110) surfaces amounts to –96% as measured by ECS. The ESP found at single-crystalline surfaces of hcp Co is positive or negative, depending on the one-dimensional densities of state for Co, whereas the ESP at surfaces of bcc Fe is always positive in agreement with band structure calculations. These findings show the importance of investigating single-crystalline surfaces, and correlating the ESP(hkl) values to the respective P(hkl) values derived from band structure calculations. It is interesting to note that the *topmost* surface layer of the (100) surface of bulk antiferromagnetic Cr exhibits LRFO and the *topmost* surface layer of the (100) surface of bulk paramagnetic V also exhibits LRFO as found by ECS in agreement with theoretical predictions [11, 13].

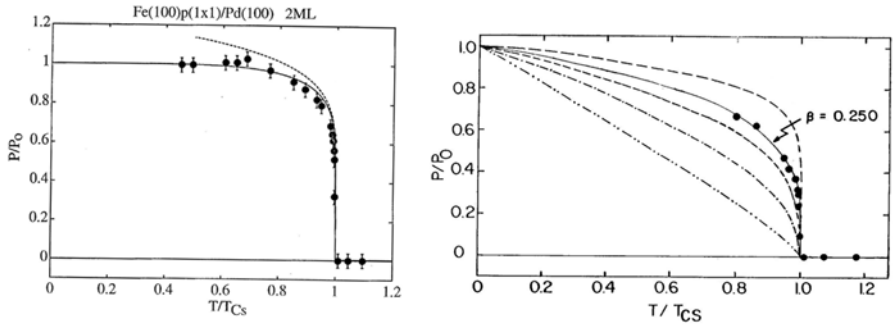

Fig. 2: (a) (left) ESP P/P_0 as function of T/T_{Cs} at the surface of a 2 ML thin bct Fe(100)p(1×1)/Pd(100) film. The solid and dashed lines represent, respectively, the exact solution of the 2D Ising model and the power law approximation for $T \to T_{Cs}$; (b) (right) ESP $P(T)$ for a 2 ML thick bcc Fe(100) film on fcc Au(100) as function of T/T_{Cs}. The lines represent theoretical predictions for M of the 2D Ising model (—-), the 3D Ising model or the isotropic XY and Heisenberg models (- - -), the bulk mean-field model (-.-.-.-), and of the surface transition of the Heisenberg model (-..-..-).

ECS was utilized to study the existence of LRFO at surfaces of ultra-thin (1–4 ML) bct Fe(100)/fcc Pd(100) films [14]. In Fig. 2a, the temperature (T) dependence of the ESP P/P_0 at the surface of 2 ML thin bct Fe(100) films on Pd(100) is given as function of T/T_{Cs}, with $T_{Cs} = 613.1$ K and $P_0 = -33\%$ the calculated ESP at $T = 0$. The full line in Fig. 2a represents the T-dependence of M as predicted by Yang [15] for the 2D Ising model. The dashed line in Fig. 2a gives the asymptotic power law approximation. T_{Cs} and the critical exponent β

are determined by a linear least-square fit of the ESP data under the assumption of a power law of the form $(T_{Cs} - T)^{\beta}$ for $t = (T_{Cs} - T)/T_{Cs}$ between 0.97 and 1.0. The value of β is found to be $\beta = 0.125 \pm 0.01$. The dashed curve in Fig. 2a corresponds to $\beta = 0.125$ and fits the experimental data quite well for t between 0.97 and 1.0. The value for the critical exponent β agrees well with the exact value (1/8) of the 2D Ising model of a ferromagnet for $T \to T_{Cs}$. The ECS data are, for $0.45 \leq t \leq 1$, in excellent agreement with the T-dependence of the spontaneous M as predicted by Yang [15] for a 2D Ising magnet.

ECS was used to study bcc Fe(100)/fcc Au(100) films [22]. As for Fe(100)/Ag(100), we find, for films ranging in thickness from 1 to 3 ML, always nonzero *in-plane* ESP between 113 K and 303 K. The ECS results for a 2 ML thick bcc Fe(100)/fcc Au(100) film are shown in Fig. 2b together with theoretical predictions for various phase transition models. With increasing T, the ESP decreases monotonously from its low temperatue value of 16% at 113 K to zero at $T_{Cs} = 290.03$ K. From a logarithmic plot of the ESP as function of the reduced temperature T/T_{Cs}, T_{Cs} and the critical exponent β are determined simultaneously by a linear least-square fit of the ESP data. A power law of the form $(T_{Cs} - T)^{\beta}$ is assumed and least square fits of the data yield $T_{Cs} = 290.03 \pm 0.02$ K. For that optimal value of T_{Cs}, β is found to be 0.25 ± 0.01.

Bcc V(100)p(1x1) films are deposited at $8 \cdot 10^{-10}$ mbar on fcc Ag(100) substrates. For all film thicknesses (d = 1–7 ML), nonzero P values are observed, clearly establishing the existence of LRFO at the *topmost* layer of the films [17, 18]. Fig. 3a shows the T-dependence of the normalized long-ranged ESP P/P_0 at the surface of 5 ML thick V(100)p(1×1)/Ag(100) films as function of T/T_{Cs}, with $T_{Cs} = 475.1$ K and $P_0 = -17.8\%$ the calculated ESP at $T = 0$. T_{Cs} and the critical exponent β are determined as before. The value of β is found to be $\beta = 0.128 \pm 0.01$. This value agrees well with the exact value 0.125 of the 2D Ising model. These results are consistent with electron band calculations of Yokoyama et al. [19], of Fu et al. [20], and of Gay and Richter [21].

In Fig. 3b the T-dependence of P for 5 nm thin Tb(0001)/W(110) films is given for $H = 250$ Oe [22]. Nonzero P values establish that the existence of LRFO up to 248 K, which lies above both T_{Cb} and T_{Nb}, as indicated in Fig. 3b. Using ferromagnetic induction and Kerr effect measurements, T_{Cb} is found to be located at 220 K as shown in Fig. 3b. With increasing T, P decreases from 22% at 146 K to 7% at about 240 K, which lies slightly above T_{Cb} and T_{Nb}. As T increases further, P increases very steeply to 21% at 243 K and drops to zero at $T_{Cs} = 249.96$ K. In Fig. 3b, the T variation of P in the neighborhood of T_{Cs} is used to determine the critical exponent β. For $(T_{Cs} - T)/T_{Cs}$ ranging between $2 \cdot 10^{-2}$ and 10^{-4}, $\beta = 0.348 \pm 0.01$ is obtained.

Taking surface anisotropies into account, it is found [23] that, along an axis of easy M, β can amount to 0.35. The value $\beta = 0.35$ agrees well with our exper-

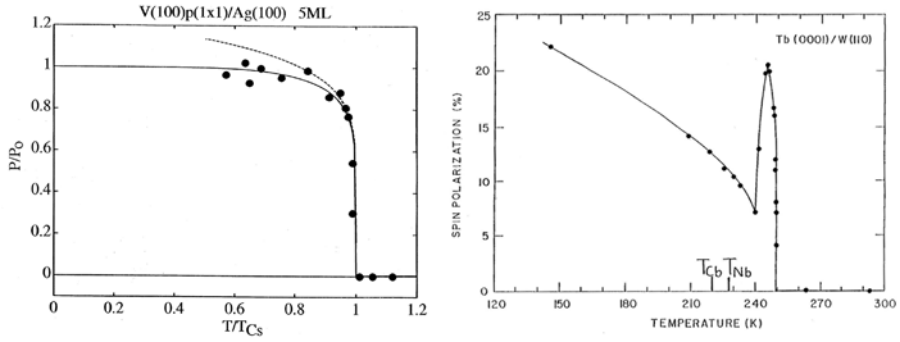

Fig. 3: (a) (left) ESP P/P_0 as function of T/T_{Cs} for a 5 ML film of bcc V(100) on fcc Ag(100). The solid and dashed lines represent, respectively, the exact solution of the 2D Ising model and the power law approximation for $T \to T_{Cs}$; (b) (right) ESP $P(\%)$ at the *topmost* surface layer of 5 nm thin hcp Tb(0001)/bcc W(110) films as function of T. T_{Cb} denotes the bulk Curie temperature and T_{Nb} denotes the bulk Néel temperature of Tb.

imental result $\beta = 0.348$ measured along an easy axis. Quite recently, Wojtczak and Rutkowski [4] calculated the T-dependence of M and find excellent agreement with the experimental data. Two electron capture ECS experiments indicate the existence of "local" SRFO up to ≈ 400 K.

For comparison, Fig. 4a gives log-log plot of ESP data obtained by using ECS at surfaces of V(100)/Ag(100), bcc Fe(100)/Au(100) and hcp Tb(0001)/W(110) films. The ESP data given in Fig. 2a for bct Fe(100)/fcc Pd(100) films are well represented by the solid line for $\beta = 0.125$. We have studied these phase transitions in more detail [24]. It is found that the nature and orientation of the substrate, here Pd(100) and Au(100), have significant effects on the ferromagnetic phase transition, in particular the thermodynamic behavior near the Curie point is strongly dependent on the details of the system, in contrast to the case of bulk Fe. It is shown that these results are consistent with predictions for the 2D XY model with two-fold and four-fold symmetry breaking crystalline anisotropies.

Using SPEES, the magnetization M, or the average ESP, is measured at surfaces of 4 ML thin Fe(100)/Pd(100) films for 150 keV H^+ ions as function of the incidence angle α (see Fig. 4b). The highest ESP value (0.37) is obtained for $\alpha < 0.6°$, where the incident ions cannot penetrate the topmost surface layer. Therefore, this ESP value should represent a measure of the surface M. A drop in the average ESP from 37% to 28% is observed when α is increased above 0.6° where the ions start probing subsurface and bulk layers. Therefore, ESP values for $\alpha > 2°$ can be related to the bulk M. This enhancement of the ESP amounts to 32%, which is in excellent agreement with theoretical predictions [20, 27]. From further SPEES experiments at 2ML thin Fe(100)/Pd(100) films, it is found that

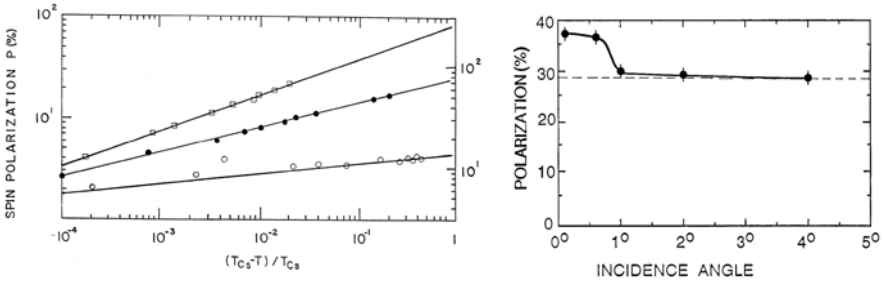

Fig. 4: (a) (left) Log-log plot of the ESP data shown in Figs. 2a, b and 3a, b. P values at the right side of Fig. 4a. 5 ML bcc V(100)/fcc Ag(100): circles, $\beta = 0.128$ and $T_{Cs} = 475.1$ K; 2 ML bcc Fe(100)/fcc Au(100): full circles, $\beta = 0.25$ and $T_{Cs} = 290.01$ K; 5 nm thin hcp Tb(0001)/bcc W(100): squares, $\beta = 0.348$ and $T_{Cs} = 249.96$ K. The solid lines are drawn for $\beta = 0.125$, 0.250 and 0.350; (b) (right) Average, layer-dependent ESP at surfaces of 4 ML thin bct Fe(100)/Pd(100) films as function of the angle of incidence α of the ions.

emitted Pd Auger electrons are spin-polarized, and that the ESP is oriented parallel to that of the Fe(MVV) Auger electrons [28].

Quite recently, we have found, for the first time, the existence of 2D LRFO at surfaces 1ML thin films of the bulk paramagnetic, 4*d*-metal Ru [29]. From Auger electron spectroscopy we find that the initial growth of Ru on a C(0001) substrate is lateral until a homogeneous monolayer film is formed. The magnetic properties of the films are studied using SPEES with 3 keV electrons. For 1 ML of hcp Ru on hcp C(0001), below $T_{Cs} \approx 250$ K, nonzero in-plane P is observed and found to saturate in an applied field of a few tenths of an Oe [29].

Presently, nano- and micron-sized magnetic elements are being explored for their practical use for ultra-high density magnetic storage, for magnetic reading and writing heads and for magnetic sensor arrays. In their study to explain switching field fluctuations of patterned magnetic elements, Zheng and Zhu [30] reported on two remanent magnetization patterns of Co elements, so-called "C" and "S" states. We have used SIMPA to investigate the magnetic structure of "C" and "S" states at surfaces of 30 nm thin, focused ion beam (FIB) patterned, polycrystalline Co elements on Si(100) substrates [12]. Fig. 5a shows a SIMPA spin map of a magnetic Co element. The density of the P vectors (white arrows in Fig. 5a) is reduced by a factor of 16 in order to give a clear plot. From this plot, the existence of a magnetic "S" state is clearly visible. The grey shades in Fig. 5a represent different orientations of the in-plane P as given by the grey shade wheel shown in the right part of Fig. 6. Fig. 5b shows a magnetic image of a circular magnetic element (20 μm diameter) created by FIB milling from a 30 nm thick Co/Si(100) film. The "C" shaped magnetization configuration can be easily seen from the orientation of the P vectors (black arrows in Fig. 5b).

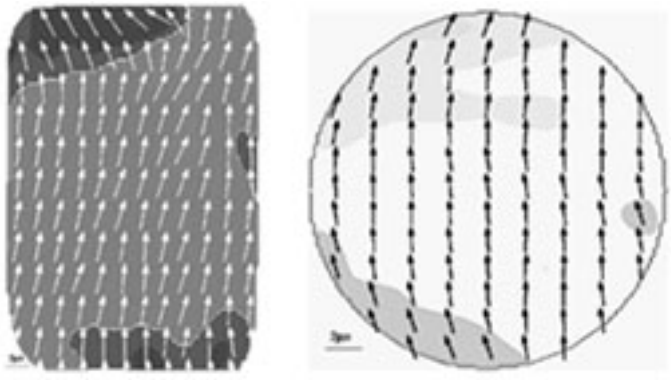

Fig. 5: (a) (left) SIMPA spin map of a focused ion beam (FIB) created magnetic Co element (thickness 30 nm) of size 30 μm$\times$21 μm with rounded edges; (b) (right) SIMPA spin map of a circular (20 μm diameter) FIB created Co element. For this image, the grey shade wheel (see right part of Fig. 6) is slightly rotated to enable a simplified identification of the "C" state.

Fig. 6 shows a spin map obtained at the surface of a circular, FIB created magnetic Co/Si (100) element (35 μm diameter). The local orientation and magnitude of the P vectors are given by white arrows. From the distribution of the P vectors it is clearly visible that the surface ESP is non-uniform. The curling of the P vectors shows the existence of magnetic vortex and anti-vortex states [31], which directly illustrates that such states have to be considered in realistic calculations of magnetization reversal mechanisms.

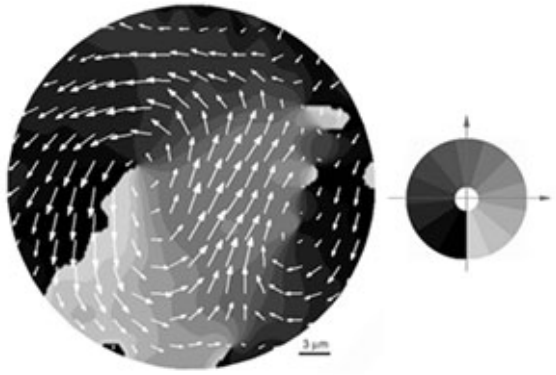

Fig. 6: SIMPA spin map of a circular (35 μm diameter) Co/Si(100) element. A grey shade wheel is given in the right part of the figure.

Magnetic phenomena such as magnetic couplings (MC) between two ferromagnetic layers through a magnetic or non-magnetic spacer layer receive great

attention [6]. We report on detailed studies of spin-resolved domain and domain wall structures of wedged bct Fe(100)(35 ML)/Mn/bct Fe(100)(50 ML) films deposited pseudomorphically on surfaces of Pd(100) substrate crystals as function of Mn spacer layer thickness d_{Mn}, which is varied from 1 ML to 9 ML.

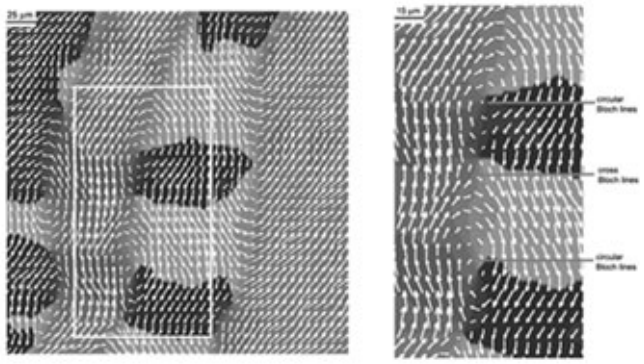

Fig. 7: (a) (left) SIMPA spin map of the surface of a bct Fe(35 ML)/Mn/bct Fe(50 ML) film for $d_{\mathrm{Mn}} = 3$ ML. depicting many cross-tie-like magnetic patterns with circular and cross Bloch lines; (b) (right) Enlarged SIMPA spin map of the area marked in (a).

Without MC, the P vectors in the surface domains should be aligned along one of these easy axes of bct Fe(100). Already for $d_{\mathrm{Mn}} = 1$ ML, besides 180° and 90° domain walls, also 70° domain walls are found. It is obvious that the competition between magnetocrystalline anisotropy and canted MC [32, 6] causes the 70° angle between the P vectors at the 70° wall, which gradually increases to 90°, becoming aligned along an ⟨100⟩ easy axis of bct Fe(100). Fig. 7a shows a SIMPA spin map for $d_{\mathrm{Mn}} = 3$ ML. A grey shade wheel is given in the right part of Fig. 6. The curling of the P vectors is stronger and more non-uniform. Fig. 7a shows many cross-tie-like magnetic patterns with circular and cross Bloch lines, making the distinction between domains and domain walls less pronounced and indicating, from the reduced magnitude of the P vectors in the center of the circular and cross Bloch lines, the existence of nonzero P components pointing out of the surface plane. For easy identification of the cross-tie like magnetic patterns, in Fig. 7b an enlargement spin map of the area marked in Fig. 7a is presented, showing one cross-tie like pattern with 1 cross and 2 circular Bloch lines, which obviously results from the collapse of a 180° domain wall. From the SIMPA experiments, there is strong evidence that the MC is non-collinear (canted).

The new spin-sensitive spectroscopies, ECS, SPEES and SIMPA, permit very selective investigations of surface magnetic structures and promise to reveal many new and exciting phenomena in the future. The data, they provide, will present a continuing challenge to theoretical models on macro-, micro- and nano-magnetic

properties of magnetic systems. The experiments, discussed here, provide clear evidence that ECS, SPEES and SIMPA are powerful techniques to study *topmost* surface and interface layer magnetic properties.

References

[1] A. J. Freeman, C. L. Fu, in: *Magnetic Properties of Low-Dimensional Systems*, Eds. L. M. Falicov, J. L. Morán-López (Springer Proceedings in Physics, Vol. 14, Springer, Berlin, 1986)

[2] H. W. Diehl, in: *Phase Transitions and Critical Phenomena*, Eds. C. Domb, J. L. Lebowitz (Academic, London, 1986), Vol. 10

[3] A. Hubert, R. Schäfer, *Magnetic Domains: The Analysis of Magnetic Microstructures* (Springer, Berlin, 1998)

[4] L. Wojtczak, J. Rutkowski, J. Magn. Magn. Mater. **148** (1995) 72

[5] *Phase Transitions and Critical Phenomena*, Eds. C. Domb, J. L. Lebowitz (Academic, 1983)

[6] J. Li, C. Rau, J. Magn. Magn. Mater. (2004) in print

[7] C. Rau, R. Sizmann, Phys. Lett. A **43** (1973) 317

[8] C. Rau, J. Magn. Magn. Mater. **30** (1982) 141

[9] C. Rau, K. Waters, N. Chen, Phys. Rev. Lett. **64** (1990) 1441

[10] N. J. Zheng, C. Rau, Mat. Res. Soc. Symp. Proc. **313** (1993) 723

[11] C. Rau, S. Eichner, Phys. Rev. Lett. **47** (1981) 939

[12] J. Li, C. Rau, J. Appl. Phys. **95** (2004) 6527

[13] C. Rau, C. Liu, A. Schmalzbauer, G. Xing, Phys. Rev. Lett. **57** (1986) 2311

[14] C. Rau, P. Mahavadi, M. Lu, J. Appl. Phys. **73** (1993) 6757

[15] C. N. Yang, Phys. Rev. **85** (1952) 808

[16] C. Rau, C. Jin, G. Xing, Phys. Lett. A **144** (1990) 406

[17] C. Rau, C. Schneider, G. Xing, K. Jamison, Phys. Rev. Lett. **57** (1986) 3221

[18] J. Balberg, J. S. Helman, Phys. Rev. B **18** (1986) 303

[19] G. Yokoyama, N. Hirashita, T. Oguchi, T. Kambara, K. I. Gondaira, J. Phys. F **11** (1981) 164

[20] C. L. Fu, A. J. Freeman, T. Oguchi, Phys. Rev. Lett. **54** (1985) 2700

[21] J. G. Gay, R. Richter, Phys. Rev. Lett. **56** (1986) 2728

[22] C. Rau, C. Jin, M. Robert, Phys. Lett. A **138** (1989) 334

[23] H. W. Diehl, E. Eisenriegler, Phys. Rev. B **30** (1984) 300

[24] C. Rau, M. Robert, Mod. Phys. Lett. B **10** (1996) 223

[25] C. Rau, N. J. Zheng, M. Lu, J. Magn. Magn. Mater. **121** (1993) 163

[26] C. Rau, Prog. Surf. Sci. **46** (1994) 135

[27] J. W. Krewer, R. Feder, Physica B **172** (1991) 135

[28] C. Rau, M. Lu, N.J. Zheng, in: *New Trends in Magnetism, Magnetic Materials, and Their Applications*, Eds. J. L. Morán-López, J. M. Sanchez (Plenum, New York, 1994) p. 195

[29] R. Pfandzelter, G. Steierl, C. Rau, Phys. Rev. Lett. **74** (1995) 3467

[30] Y. Zheng, J.-G. Zhu, J. Appl. Phys. **81** (1997) 5471